Astron. Astrophys. 345, 521–530 (1999)

ASTRONOMY AND ASTROPHYSICS

# BVRI photometry of the star-forming region NGC 2264: the initial mass function and star-forming rate⋆

**E. Flaccomio**[1], **G. Micela**[2], **S. Sciortino**[2], **F. Favata**[3], **C. Corbally**[4], **and A. Tomaney**[5]

[1] Dipartimento di Scienze Fisiche ed Astronomiche – Università di Palermo
[2] Osservatorio Astronomico di Palermo G.S. Vaiana, Palazzo dei Normanni, I-90134 Palermo, Italy
[3] Astrophysics Division – Space Science Department of ESA, ESTEC, Postbus 299, 2200 AG Noordwijk, The Netherlands
[4] Vatican Observatory Research Group, University of Arizona, Tucson, AZ 85721, USA
[5] Department of Astronomy, Columbia University, New York, NY, USA

Received 1 September 1998 / Accepted 29 January 1999

**Abstract.** The pre-main sequence (PMS) population in the mass range between $\approx 0.2$ and $\approx 3\,M_\odot$ in southern part of the star-forming region NGC 2264 has been studied, determining both the Initial Mass Function in the region as well as the star-formation rates for different mass ranges. The sample is a composite one, derived through the union of samples obtained through different techniques and each suffering from different biases: previously known PMS stars in the region from the literature, photometrically-selected T Tauri candidates (from our own photometric data, discussed in detail in the present paper) and X-ray selected PMS candidates (discussed in detail in a companion paper) have been joined to form a sample which we show to be statistically complete (i.e. free from the biases which affect each of the parent samples) down to $\simeq 0.6\,M_\odot$ (while being incomplete at lower masses). Individual masses and ages have been derived by placing the individual stars on evolutionary tracks, allowing us to derive both the IMF and the star formation rate.

The Initial Mass Function thus derived for NGC 2264 shows evidence for a bimodal distribution of masses, with a break in the IMF at around $1\,M_\odot$.

**Key words:** Galaxy: open clusters and associations: individual: NGC 2264 – stars: pre-main sequence – stars: late-type – stars: formation

## 1. Introduction

Star-forming regions (SFRs) have always been the ideal laboratory for the study of the mechanisms of stellar formation, as well as for the study of the structure and time evolution of newly formed stellar systems from the early pre-main sequence (PMS) phase down to the young main sequence (MS). In spite of the several advances which have been made possible by the availability of new spectral domains (and notably of the soft X-ray band), and of the large attention which they have received in the recent literature, several key questions regarding the mechanisms of star formation are still unanswered, both from an observational as well as from a theoretical point of view.

In particular, the key issue of whether star formation is essentially an universal, self-regulating process (thus leading to an universal initial mass function – IMF) or whether its outcome depends strongly on the local conditions and/or on the triggering event which started the collapse of the original cloud (which would result in different IMFs for different regions) is still unsolved. The derivation of the IMF, as well as of the star-formation rate in different SFRs with different observed conditions supplies an important constraint to whether star formation is an universal process or not.

At a distance of about 760 pc (Sung et al. 1997)[1], and at an estimated age varying between $3 \times 10^6$ years (Walker 1956; Mermilliod 1981) and $10^7$ years (Sagar et al. 1986), the star forming region NGC 2264 allows us to study the earlier stages of stellar evolution.

The disadvantage of its larger distance with respect to other well studied regions with similar characteristics (e.g. the Taurus-Auriga or Orion clouds) is compensated by two facts, which greatly ease the interpretation of the observational data: a small *interstellar* visual absorption ($\mathrm{E(B-V)} = 0.06$ mag.; Pérez et al. 1987) for the cluster members and the presence, in the immediate proximity of the region, of an optically thick reflection nebula (see e.g. Herbig 1954) that effectively obscures background stars.

Fig. 1 shows a photographic image (taken from the STScI Digital Sky Survey) of the central part of NGC 2264, in which the presence of the cloud is clearly revealed by the distinct decrease in the surface density of stars toward the area around and between the two brightest stars of the association: S Mon (north) and W178 (HD47887, south). It can also be seen that,

*Send offprint requests to*: Ettore Flaccomio (ettoref@oapa.astropa.unipa.it)

⋆ Based on observations with the VATT: the Alice P. Lennon Telescope and the Thomas J. Bannan Astrophysics Facility. Table 3 is available in electronic form at CDS via ftp 130.79.128.5

[1] Although the earlier study of Pérez et al. (1987) estimated the distance at 950 pc

**Table 1.** Optical characteristics of the VATT telescope.

| | |
|---|---|
| Optical system | aplanatic Gregorian, f/9 |
| Focal length | 16.48 m |
| Primary mirror | f/1.0, 1.83m. diameter |
| Secondary mirror | f/0.9, 0.38m. diameter |
| Vignetting-Free Field | 72 mm diameter (15 arcmin) |
| Image scale | 12.52 arcsec/mm |
| Image quality | 0.1 arcsec within 6.8 arcmin from axis |
| Mounting | altitude-azimuthal with derotator |

contrary to most stellar associations that show a single clustering of stars, NGC 2264 has a rather complicated spatial structure: we can identify two physically distinct agglomerations, one to the North and one to the South (see Sagar et al., 1988).

Since the classical study of Walker (1956) suggested that a large fraction of the stars in the area are in the pre-main sequence stage, several workers have tried to characterize the stellar population of the region, using different techniques. Proper motion studies (Vasilevskis et al. 1965), X-ray observations (Simon et al. 1985, Patten et al. 1994, Flaccomio et al. in prep.), $H\alpha$ surveys (Herbig 1954; Ogura 1984; Marcy 1980; Sung et al. 1997), IRAS infrared imaging (Margulis et al. 1989) and photometric studies (Adams et al. 1983; Rydgren 1979; Lada et al. 1993) have progressively enriched the knowledge of the young stellar population of NGC 2264.

The identification of the optical counterparts of a deep X-ray survey of NGC 2264 using the ROSAT HRI instrument recently conducted by Flaccomio et al. (in prep.) shows that the existing studies of the region do not provide an unbiased list of members down to sufficiently faint magnitudes. Therefore, CCD observations of part of the region in the Johnson-Cousin BVRI bands were conducted, covering the 20 arcmin square shown in Fig. 1. The area, which is roughly centered on the bright B1.5 V star W178, includes a good part of the southern star-forming core as well as the characteristic cone nebula.

The observations and their reductions are discussed in Sect. 2 of the present paper, while the results obtained are presented and discussed in Sect. 3, and summarized in Sect. 4.

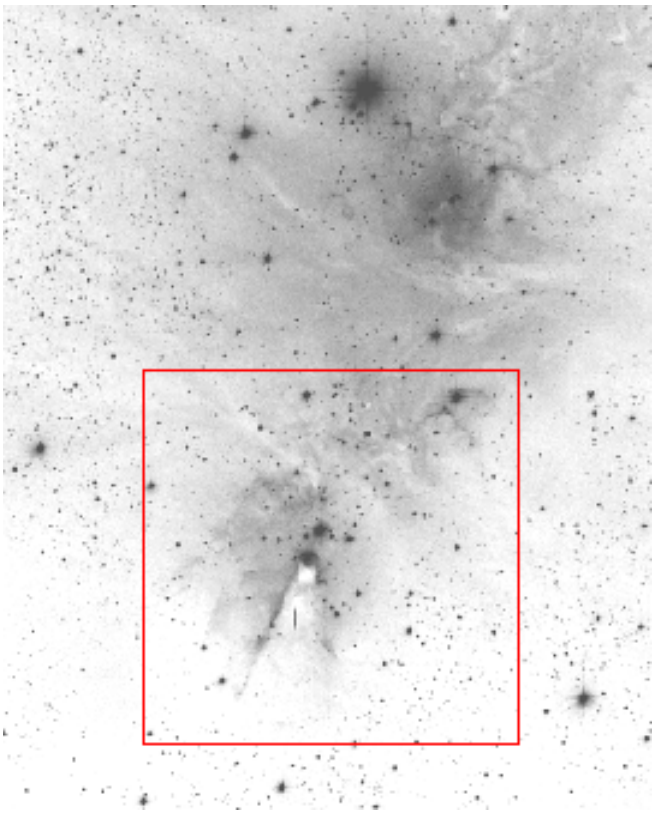

**Fig. 1.** An image of NGC 2264 from the STScI Digital Sky Survey. The square (20 arcmin on a side) indicates the extent of the CCD frames which are discussed in the present paper. Note the distinct decrease in star density toward the center of the region due to the presence of the molecular cloud. North is up, east to left.

## 2. Observations and data reduction

### *2.1. Instrumentation and observations*

The CCD frames discussed here were acquired at the Vatican Advanced Technology Telescope (VATT) on Mt. Graham, in Arizona, using the Columbia SpectraSource CCD camera, during the nights of December 2 and 3, 1996. The conditions were photometric during both nights. A short summary of the optical characteristics of the telescope is given in Table 1. The CCD was a 2048 pixel square Tektronic chip. At the plate scale of the VATT, each pixel spans about 0.33 arcsec in the sky, yielding a square field of view of about 11 arcmin on a side. The filters used closely reproduce the standard passbands of the Johnson-Cousin B, V, R and I filters.

The square field shown in Fig. 1 was surveyed with a mosaic made with four different and partially overlapping pointings. Each of the four fields has been observed with the four filters and with four different exposure times, ranging from 1 to 200 seconds, in order to enhance the dynamic range of the measurements preventing the saturation of the CCD. A total of 64 CCD frames were thus obtained, in addition to the standard calibration frames and to observations of 19 standard stars from Landolt (1992). A list of the CCD frames analyzed here is shown in Table 2.

### *2.2. Data reduction and photometry*

The reduction of the data was performed using the IRAF software and in particular the tasks provided in the CCDRED package. At the time of the observations discussed here the VATT was not yet fully operational, and in particular the collimation of the optics was still being worked on. As a result, the optical quality of the individual CCD frames is not ideal, and several different approaches were explored to flat-field the data and to determine the shutter travel time. To optimally reduce the data, use was made of the program frames in addition to the calibration frames. The data reduction process is discussed in detail in Flaccomio (1996).

**Table 2.** Summary of observed fields

| Date | Type | Ra | Dec | $T_{exp}(sec)$ | Filter | $N_{tot}$ |
|---|---|---|---|---|---|---|
| 2 Dec. | Object | 6:41:27.4 | 09:21:24 | 100,10,2,1 | VRI | 12 |
| | ” | ” | ” | 200,20,2,1 | B | 4 |
| | ” | 6:41:27.4 | 09:31:24 | 100,10,2,1 | VRI | 12 |
| | ” | ” | ” | 200,10,2,1 | B | 4 |
| | Standard | 9:21:28.0 | 2:46:06 | 2–10 | BVRI | 8 |
| | ” | 6:51:29.0 | -0:16:05 | 2–10 | BVRI | 8 |
| | ” | 5:57:55.0 | -0:09:07 | 5–10 | BVRI | 4 |
| | Dome Flat | | | 5–9 | BVRI | 16 |
| 3 Dec. | Object | 6:40:46.9 | 09:21:24 | 100,10,2,1 | VRI | 12 |
| | ” | ” | ” | 200,20,2,1 | B | 4 |
| | ” | 6:40:46.9 | 09:31:24 | 100,10,2,1 | VRI | 12 |
| | ” | ” | ” | 200,20,2,1 | B | 4 |
| | Standard | 7:27:29.0 | -1:59:56 | 2–10 | BVRI | 8 |
| | ” | 5:57:55.0 | -0:09:07 | 2–10 | BVRI | 8 |
| | Dome Flat | | | 5–10 | BVRI | 16 |
| | Bias | | | 0 | | 6 |
| | Dark | | | 900–6900 | | 19 |
| | Twilight Flat | | | 1–35 | BVRI | 16 |
| | | | | | Total number of images | 173 |

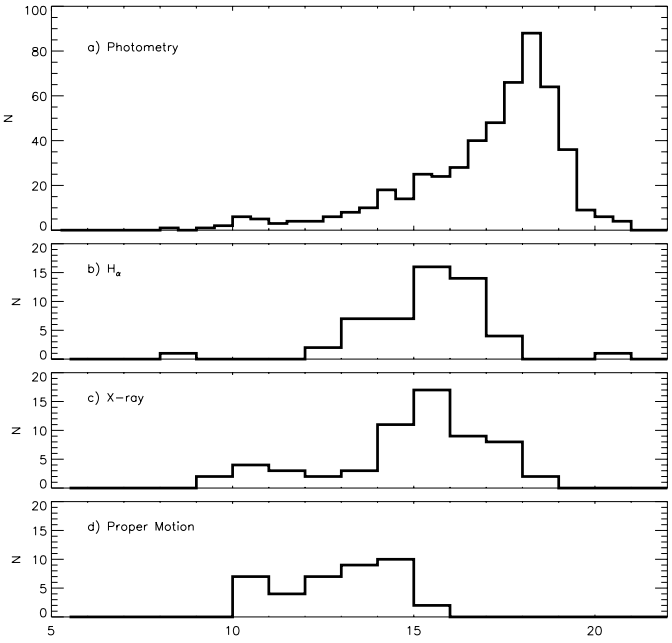


**Fig. 2a–d.** V magnitude distribution of the complete star sample in NGC 2264 discussed here (a) and of three subsample obtained by cross-identification with other catalogs from the literature (a,b,c; see text).

The ‘daofind’ source detection algorithm was used to detect individual stars in each frame, as well as to determine their position. An analysis of the magnitude distribution of the detected sources (Fig. 2a) shows that the detected sample is complete down to magnitude $V \simeq 18$, with completeness falling rapidly at the fainter magnitudes. We have also established that this completeness limit is quite uniform over our field of view by variously dividing the whole area in several sections and repeating the same kind of semi-quantitative analysis.

The magnitude of each star in the field of view was determined through synthetic aperture photometry, using the IRAF ’daophot’ package, using a circular aperture with a radius of 5 arcsec, and a background determined from a 3.3 arcsec wide concentric annulus whose inner radius was 8.3 arcsec. Each program star was then checked for contamination from nearby visible and resolved stars. The instrumental magnitudes thus obtained were converted to the Johnson-Cousin system through the use of the Landolt (1992) photometric standards.

The residuals of the transformations indicate, for stars brighter than $V = 16$, a photometric precision of better than 0.05 mags for a single measurement in each of the bands. In the vast majority of cases, we averaged the results obtained for the same star from all the available frames, leading to an estimated final uncertainty on the resulting magnitudes of 0.05 mags at $V = 17$.

We compared our magnitudes with those of Sung et al. (1997) for the 70 stars in common between the two studies. The median differences (this work vs. Sung at al. 1997) in the B, V and I magnitudes are $-0.040 \pm 0.001$, $-0.016 \pm 0.001$ and $0.024 \pm 0.001$ respectively.

The results of the photometry are summarized in Table 3 where the columns represent, in order: a running identification number, the sky coordinates of the object, and the derived magnitudes. A colon beside the identification number indicates those stars whose photometry is uncertain, in most cases because of contamination from nearby stars.

We then proceeded to cross-match our star list with the lists of probable members of NGC 2264 from various works in the literature. This yielded a list of 110 stars in common between our list and those of the examined papers: 52 of these stars are suspected of belonging to the SFR on the basis of their $H\alpha$ line emission and appear in the lists of either Herbig (1954), Marcy (1980), Ogura (1984) or Sung et al. (1997); another 39 stars have, according to the proper motion study by Vasilevskis et al. (1965), membership probabilities greater than 50%. Finally, 61 of our stars were found to be strong ($30.2 \lesssim \log L_X \lesssim 31.2$) X-ray emitters by Flaccomio et al. (in prep.). Distributions of V magnitude for these three samples are given in Fig. 2b,c,d.

## 3. Results

### *3.1. Color-color diagrams*

PMS stars are known to present several spectral peculiarities, both in their absorption/emission lines and in their overall spectral energy distribution (SED). While classical T-Tauri stars (CTTS) show strong deviations from the spectral energy distribution of normal stars, as well as strong emission lines, weak-line T-Tauri stars (WTTS), as their name implies, show little or no such peculiarities (Walter et al. 1988).

The SED of classical T-Tauri stars is usually characterized by non-photospheric excesses both in the optical/ultraviolet (the so called ‘veiling’) as well as in the infrared spectral regions.

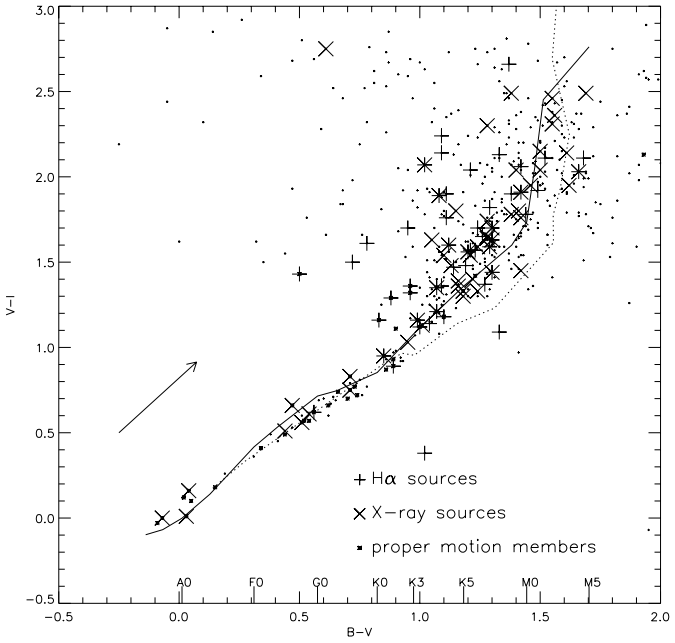


**Fig. 3.** $\mathrm{V-I}$ vs. $\mathrm{B-V}$ diagram for the stars in the NGC 2264 region observed in the present program. The solid and dotted lines respectively indicate the loci of the main sequence and of the giant branch. X-ray, $\mathrm{H}\alpha$ and proper motion selected members (see the text for details) are indicated by different symbols. The arrow indicates the reddening vector.

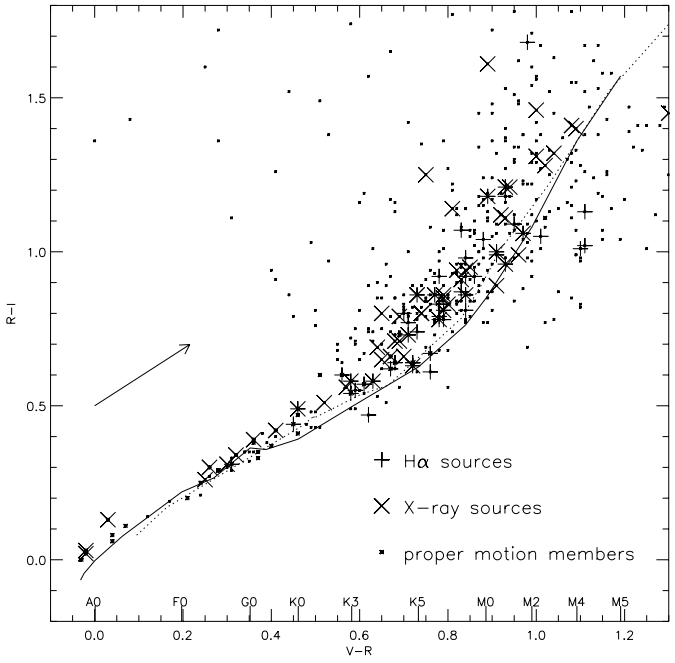


**Fig. 4.** $\mathrm{R-I}$ vs. $\mathrm{V-R}$ diagram. The meaning of symbols and curves is as in Fig. 3.

Both types of excess have been successfully related to the emission of accretion disks (e.g. Bertout et al. 1988).

While the infrared excesses due to the presence of accretion disks usually show up at larger wavelengths than those observed here, the blue contribution due to the hot accreting area is known to be extend significantly down to, at least, the V photometric band (see Hartigan et al. 1995).

Such photometric excesses will cause the star to deviate, in a color-color plot, from either the main-sequence or the giant locus. We have thus used the position of our stars in the $\mathrm{V-I}$ vs. $\mathrm{B-V}$ and $\mathrm{R-I}$ vs. $\mathrm{V-R}$ planes to select likely PMS stars. Clearly such selection procedure is presumably biased toward CTTS and, in particular, toward the youngest and most actively accreting ones.

The color-color diagram shown in Fig. 3 indeed shows that a large fraction of the redder objects deviate from both the main sequence and the giant loci. These deviations are most likely due to blue excesses in the spectra of these objects and strongly suggest their CTTS nature. This last point is reinforced by the evidence that most of the stars whose $\mathrm{H}\alpha$ line was detected in emission by Herbig (1954), Marcy (1980), Ogura (1984) and Sung et al. (1997) are seen to deviate on average more than the X-ray sources (Flaccomio et al. in prep.): while the former are mostly CTTS, the latter are, more likely, dominated by WTTS having less or no blue excess.

Fig. 4 shows a color-color diagram computed using "redder" colors than the ones used in Fig. 3; such a diagram is thus less affected by the blue excesses that were so evident in Fig. 3. Nevertheless, a numbers of stars still deviate from both the dwarf and the giant sequences.

Considering that field stars are prevalently MS objects (with possibly a few giants) those stars that lie significantly above either the Main Sequence in Fig. 3 or the giant locus in Fig. 4 are, as already suggested, likely to be classical T-Tauri stars and consequently members of NGC 2264.

The position of the few stars below and to the right of the lower of the sequences (i.e. the MS in Fig. 4 and the giant locus in Fig. 3) can be explained assuming a larger than average reddening. As the cloud right behind NGC 2264 can be considered *totally* opaque, the most plausible possibility is that these object are NGC 2264 members either with a high *circumstellar* absorption or partially embedded in the cloud. Foreground stars indeed should be even less reddened than the average 'interstellar' NGC 2264 value of $\mathrm{E}(B-V)=0.06$, so that they should remain close enough to the MS not to be mistaken for cluster stars.

Following the previous discussion, we chose to select as NGC 2264 members those stars that, in one or both of the color-color diagrams, are more distant from the region bounded by the MS and the giant locus than the photometric uncertainties would allow. Considering only stars brighter than V=17, whose photometric error can be quite reliably estimated (i.e. 0.1 mag. in both axis, with a $2\sigma$ confidence) we thus selected 46 likely members, 24 of which were previously unknown.

Although this selection criterium has resulted in a significant number of new members of the population of NGC 2264, the procedure adopted has no claim of completeness (as it is true for the other membership criteria). Inspection of the color-color diagrams shows that known members with earlier spectral types do not show any photometric excesses, and thus that the adopted procedure preferentially selects later spectral types.

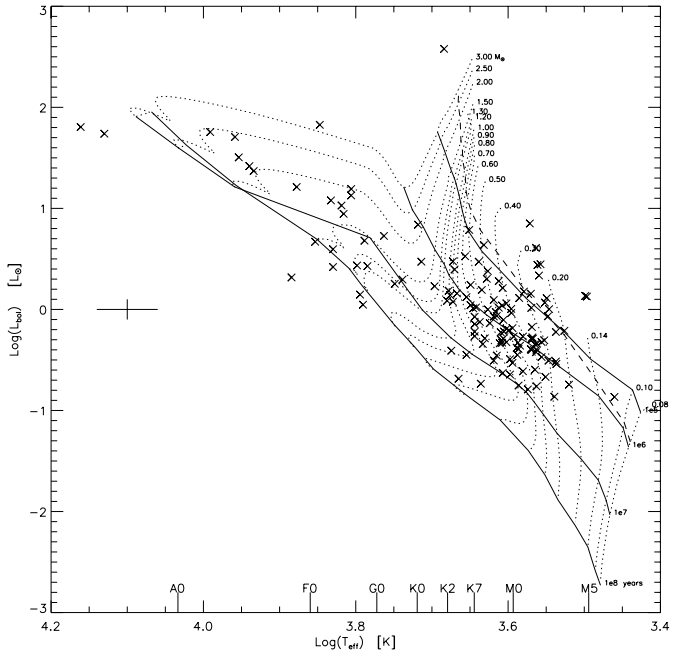


**Fig. 5.** H-R diagram of the photometrically-selected NGC 2264 members. Evolutionary tracks and isochrones from D'Antona & Mazzitelli (1998) are shown. The dashed line indicates the deuterium burning locus and the cross on the left side of the diagram indicates typical uncertainties.

### *3.2. The membership catalog*

Our NGC 2264 membership catalog, containing 141 members, is shown in Table 5. The first column refers to the identification number in Table 3. A colon besides this numbers signals an uncertain photometry. We then list the sky position, photometry and derived physical parameters of the selected stars (see Sect. 3.3). The column labeled "Memb" indicates the methods by which each star was selected. The letters indicate: 'c', stars selected because of their colors using the method discussed above; 'x', the counterparts of the X-ray sources listed by Flaccomio et al. (in prep.); 'h', the H$\alpha$ stars from the catalogs of Herbig (1954), Marcy (1980), Ogura (1984) and Sung et al. (1997); 'p', the proper motion stars from Vasilevskis et al. (1965) with membership probabilities greater than 50%. The last column shows the result of the cross identifications.

Excluding the list by Sung et al. (1997), which include only stars in the northern half of our field of view ($\mathrm{RA} \gtrsim 9.5$), all of the other surveys entirely cover the area of the sky we study in this paper. Anyway, none of these (largely overlapping) samples is complete: Vasilevskis et al. (1965) proper-motion survey has a magnitude limit of $V \simeq 15$, the H$\alpha$-selected samples are strongly biased toward the CTTS population, as is our photometrically selected sample. The X-ray sample, which is also the largest, is likely to include both CTTS and WTTS. It also spans a larger range of spectral types than all the other samples but it is biased toward the more active stars.

We will show in the next subsection that, in building the Mass Function for the observed part of NGC 2264, the different biases actually compensate each other to some degree and that the union of these samples reaches near completeness, at least for the most massive stars ($\mathrm{M} \gtrsim 0.6\,\mathrm{M}_\odot$).

### *3.3. The H-R diagram*

Fig. 5 shows the H-R diagram for the stars selected as NGC 2264 members, superimposed on the pre-main sequence evolutionary tracks from D'Antona & Mazzitelli (1998). Bolometric luminosities for each star were derived from our photometric data using the Bessel & Stringfellow (1993) $\mathrm{BC_I}$ vs. $V-I$ relation and assuming a distance of 760 pc; effective temperatures were calculated from the (de-reddened) V−I for stars with $(\mathrm{V}-\mathrm{I})_\mathrm{o} > 0.0$, and from $(\mathrm{B}-\mathrm{V})_\mathrm{o}$ for the bluer ones. In the first case we employed the Schmidt-Kaler (1982) color-temperature relation adapted with the aid of the Bessel (1990) color-color relation. In the second we used the Code et al. (1976) relation. A correction for mean reddening (Pérez et al. 1987) was applied to the photometry prior to these calculations.

Although we adopted a distance of 760 pc (Sung et al. 1997), a wide range of distance estimates are available in the literature for NGC 2264. Pérez et al. (1987), for example, observationally derived individual extinction laws for each star, finding evidence of anomalous reddening, and obtaining a distance of 950 pc, higher than most available distance estimate. Our adopted distance however, other than being the most recently obtained value, is also close to the average of all modern estimates.

In the determination of both the bolometric luminosity and the effective temperature of low mass stars we used the $V-I$ color indices and $I$ magnitudes, which better represent the photospheric emission of PMS stars (Kenyon & Hartmann 1990; Sung et al. 1997). Individual differential reddening and residual color excesses may however introduce competing systematic shifts in the effective temperature and bolometric correction for each star. Other sources of uncertainty for the luminosity and/or temperature determination are the possible presence of unresolved companions and, for CTTS, the occultation of part of the photosphere by circumstellar disks (see e.g. Kenyon & Hartmann 1990). The apparent positions of the few stars that lie over the birthline in the H-R diagram may well be explained by these systematics. The mass and age of individual stars were thus estimated by their positions on the D'Antona & Mazzitelli (1998) evolutionary tracks. Five stars in Fig. 5 appear to lie below the main sequence. For the four of these stars closest to the main sequence we assumed the mass of the closest evolutionary track and the age of $10^8$ years, we have discarded the remaining one.

### *3.4. Dynamical Evolution and Mass Segregation*

The area of the sky we study in this work does not cover the entire Star Formation Region (see Fig. 1) but only its southern part around the bright star W178. Our result can thus only be strictly valid for this region.

If the association has undergone significant dynamical evolution the observed mass and age spectra of our sample may differ from the initial distributions that we intend to study. Moreover, as indicated by several studies (see e.g. Sagar et al., 1988; Raboud & Mermilliod, 1998), mass segregation is also present in young clusters with ages smaller than their relaxation time. This fact has been interpreted as a result of inhomogeneous formation conditions within the cloud leading the concentration of massive stars toward its center.

We thus tried to study the spatial distribution of stars in relation to stellar mass. A quantitative study is made rather problematic by the difficulty of defining a cluster center for NGC 2264. Sagar et al. (1988), for example, define two centers, one corresponding to the bright star S Mon, north of our surveyed region, the other close to the star W157 (our star 339 in Table 5).

No clear mass segregation is apparent from the spatial distribution of stars of different masses. Although this failure to detect mass segregation may be due to the small area investigated, it quite possibly reflects the actual situation. First: the relaxation time for NGC 2264, as calculated by Sagar et al. (1988) is $\mathrm{Log(T_E)} \sim 7.4$, greater than its age. Second: mass segregation in non-relaxed clusters has been usually observed only for more massive stars ($\mathrm{M/M_\odot} > 20$, Raboud & Mermilliod, 1998) than those considered; here we are interested only in the low mass ($\mathrm{M/M_\odot} < 3.0$) population of NGC 2264 and we only derive masses and ages for these stars.

### *3.5. The Initial Mass Function in NGC 2264*

In order to build a meaningful IMF it is of primary importance to take into account the completeness of the star samples used. Here we assume that, for a given stellar mass, the observational biases of the proper motion sample are not correlated with those affecting the three other samples used (i.e. the ones selected on the basis of X-ray emission, H$\alpha$ emission, and of strong color excesses). It follows that, although by itself biased toward massive stars, the proper motion sample constitutes, in each mass bin, a random sample of the whole population, free from the biases that affect the other samples. The proper motion members can therefore be used to derive the (mass dependent) selection efficiency of any of the other samples, e.g., for the X-ray sample:

$$\frac{N_{\mathrm{X}}}{N_{\mathrm{total}}} = \frac{N_{\mathrm{X\&P.M.}}}{N_{\mathrm{P.M.}}} \qquad (1)$$

where $N_{\mathrm{total}}$ refers to the total number of NGC 2264 members in the field of view, $N_{\mathrm{X}}$ and $N_{\mathrm{P.M.}}$ refer to members detected in X-rays and proper motion surveys, respectively, and $N_{\mathrm{X\&P.M.}}$ is the number of proper motion members detected in X-rays.

A similar calculation has been performed for all the considered samples (i.e. X-ray, H$\alpha$, color excess and proper motion) as well as for their union in the mass range $-0.2 \lesssim \mathrm{Log(M/M_\odot)} \lesssim 0.4$, where the proper motion sample and the other three overlap to some degree. The results are shown in Table 4. For each considered mass bin we report the expected selection efficiency of any of the methods. As expected, each sample is individually incomplete, but the union of all the samples represents reasonably well the actual NGC 2264 population in the considered mass range.

**Table 4.** Completeness estimate

| $\mathrm{Log(M/M_\odot)}$ | X | $\mathrm{H}_\alpha$ | C-C | All methods |
|---|---|---|---|---|
| $-0.15$ | 0.40 | 0.80 | 0.40 | 1.00 |
| $-0.05$ | 0.50 | 1.00 | 0.25 | 1.00 |
| 0.05 | 0.00 | 0.33 | 0.17 | 0.78 |
| 0.15 | 0.14 | 0.14 | 0.00 | 0.76 |
| 0.25 | 0.60 | 0.40 | 0.00 | 0.96 |
| 0.35 | 0.38 | 0.00 | 0.00 | 1.00 |

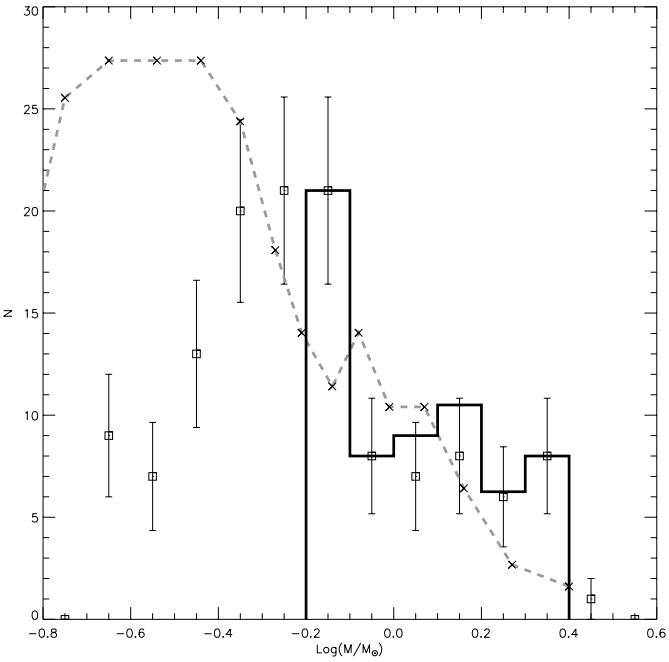


**Fig. 6.** Small squares: mass distribution for the sample of stars selected as NGC 2264 members in the present work. Error bars are simple Poisson statistics estimates (i.e. the square root of the number of stars in each mass bin). Solid line histogram: bias-corrected IMF. Dashed line: Scalo (1986) IMF with arbitrary normalization.

The resulting IMF is shown in Fig. 6; squares with error bars derived from Poisson statistics represent the actual data while the solid-line histogram, where different from zero, is the bias-corrected IMF derived as described above from the composite sample. The dashed line shows the Scalo (1986) local IMF with arbitrary normalization. While we could not estimate the completeness of our sample for $\mathrm{Log(M/M_\odot)} \lesssim -0.2$, the fall of the IMF in this mass range is most obviously due to the limiting sensitivity of both the existing data and of our survey (and thus to the incompleteness of the resulting sample) at the lower-mass end.

The resulting observational, bias-corrected IMF shows evidence for a bimodal distribution, with a "bump" in the distribution at the higher masses ($\simeq 2\,M_\odot$). We performed the KMM test (Ashman et al. 1994) to detect bimodality in an univariate data set. The test rejects with a high degree of signifi-

cance (P=0.017 or P=0.015 depending on weather we assume homoscedastic or heteroscedastic populations), the hypothesis of an unimodal distribution, thus giving support to the reality of the high mass excess. A similar result was recently obtained, for the northern part of NGC 2264, by Sung et al. (1997), who performed a study using UBVRI and H$\alpha$ photometry. The conclusions of Sung et al. (1997) are based on a list of NGC 2264 members which, due to partial spatial overlap of the two studies, has only 18 stars in common with our list, so that the two results are indeed independent.

### *3.6. Star formation history*

While individual stellar ages derived from the position of the stars on evolutionary tracks have a certain (possibly large) degree of uncertainty associated with them, because of the already discussed uncertainties on the position of the stars in the H-R diagram as well as on the tracks themselves, the relative ages (and mass attribution) should be more accurate, thus yielding a useful picture regarding the time-evolution of the star-formation rate in the region.

In Fig. 7a we have plotted the star-formation rate (defined as the number of stars with age in each logarithmic age bin divided by the size – in years – of the bin) as a function of the estimated age for our sample of stars in NGC 2264. The star-formation rate is plotted for the complete sample (square dots, with Poisson-statistics error bars) and for two subsamples segregated by mass: stars with mass greater than 1.0 $M_\odot$ with the dark continuous curve and those with $0.6 < M/M_\odot < 1.0$ with the dashed lighter one. For these latter two samples we also plot (Fig. 7b) the distribution of the logarithm of star ages. Note that both of these subsamples are within the mass range whose completeness we have shown in the previous section.

The star-formation rate for NGC 2264 shows (in any mass ranges) a steep rise in formation activity at the early stages of the history of the SFR (i.e. at large stellar ages) and a subsequent flattening. However, the presence of uncertainties in the individual age attribution would introduce such a behavior in the presence of a star-formation activity which started suddenly at some point in the past and then proceeds at constant rate. To verify this, we produced simulated star-forming rate plots under the assumption of a sudden turn-on in star formation which then proceeded at a constant rate, and with characteristic uncertainties equal to the ones we have derived from our sample. Indeed, the observed global star-forming rate for NGC 2264 is compatible with this hypothesis.

The star-formation rate for the whole sample appears to indicate an age of about $1\text{–}2 \cdot 10^6$ yr for the beginning of star formation while the two complete subsamples, which, on average, comprise more massive stars, indicate a larger age ($\sim 10^7$ yr). This fact may suggest a scenario of sequential star formation. However the total sample is very likely biased toward younger stars, as can be seen from the HR diagram in Fig. 5. The lack of low mass stars, which can likely be explained by a sensitivity limit, clearly introduces such a bias. Interestingly, however, the curve and the histogram that refer to the lower masses seem

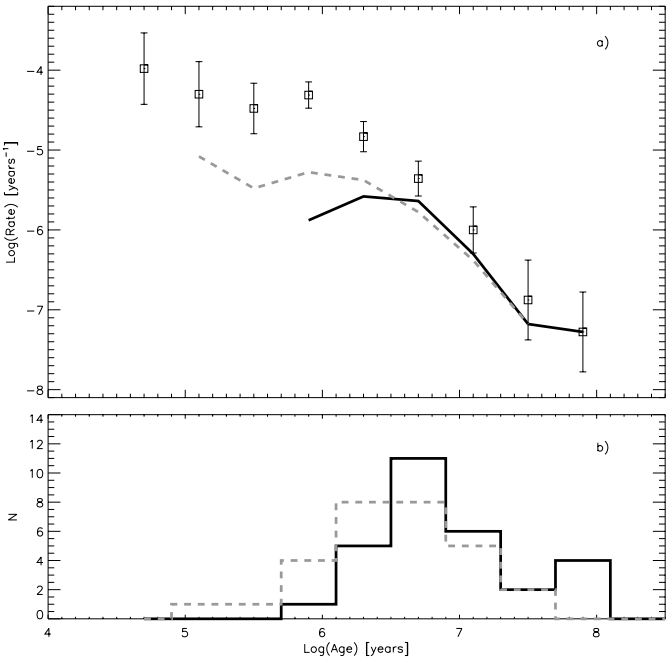


**Fig. 7. a** Star formation rate vs. age. The square dots refer to the whole sample of NGC 2264 members discussed in the present paper, with error bars derived on the basis of Poisson statistics. The two curves refer to stars with $Log(M/M_\odot) > 0.0$ and $-0.2 < Log(M/M_\odot) < 0.0$ (solid and dashed lines respectively). **b** Distribution of log(age) for the same two subsample described above.

to show a somewhat smaller typical age respect to the other one, hinting once again toward a sequential star formation. This difference in age between the two samples can hardly be considered significative, but it will be interesting, for future deeper observations, to test this hypothesis.

In any case it seems clear that star forming activity is continuing to the present day, as shown by the presence of a few stars close (or formally above) the birthline in our sample, as well as the reported presence of several very young objects in the region (e.g. Castelaz & Grasdalen 1988).

To conclude this section, we note that a sequential star formation scenario had already been suggested for NGC 2264 by Adams et al. (1983). However their proposed sequence of star formation was exactly the opposite of what is suggested by our data, starting with low mass stars and proceeding gradually with the onset of formation of more massive ones. Stahler (1985) had later reinterpreted the same data. He concluded that, due to the uncertainty in the dating of those stars that had already reached the main sequence, the observations where instead compatible with a variety of star formation histories and in particular with a contemporaneous onset of formation for all masses. Our results however are not subject to the same criticism for two reasons. First, our sample of stars is comprised of relatively low mass stars and very few of them, if any, seem to have reached the main sequence. Second, the effect described by Stahler (1985) would tend to mask, and not to produce, the kind of mass-age relation we suggest.

**Table 5.** Catalog of members.

| $N^1$ | $RA_{2000}$ h:m:s | $DEC_{2000}$ °:':" | $V$ [mag.] | $B-V$ [mag.] | $V-R$ [mag.] | $R-I$ [mag.] | $Log(L_{bol})$ $[L_\odot]$ | $Log(T_{eff})$ $[^oK]$ | $M$ $[M_\odot]$ | $Log(Age)$ [years] | $Memb.^2$ | $Ident.^3$ |
|---|---|---|---|---|---|---|---|---|---|---|---|---|
| 11 | 6:40:26.7 | 9:25:30.0 | 13.33 | 0.70 | 0.37 | 0.33 | 0.43 | 3.80 | 1.32 | 7.34 | p | V36 |
| 29 | 6:40:28.5 | 9:35:51.0 | 15.91 | 1.41 | 0.85 | 0.95 | −0.18 | 3.59 | 0.46 | 5.94 | x | W51, FX12 |
| 31: | 6:40:28.6 | 9:31: 4.0 | 14.13 | 1.19 | 0.71 | 0.77 | 0.38 | 3.63 | 0.50 | 5.38 | h | V38, O77 |
| 32 | 6:40:28.6 | 9:21:48.0 | 16.83 | 1.30 | 0.63 | 1.01 | −0.63 | 3.61 | 0.77 | 7.00 | c | |
| 33 | 6:40:28.7 | 9:21:55.0 | 13.59 | 1.87 | 1.01 | 1.01 | 0.85 | 3.57 | – | – | c | V39 |
| 50 | 6:40:30.8 | 9:34:44.0 | 15.34 | 1.23 | 0.78 | 0.79 | −0.06 | 3.61 | 0.53 | 5.92 | h | W55, S110, H12 |
| 52: | 6:40:31.1 | 9:31:10.0 | 15.16 | 1.29 | 0.73 | 0.86 | 0.02 | 3.61 | 0.49 | 5.77 | xh | W56, V41, O82, FX16 |
| 58 | 6:40:31.8 | 9:36: 4.0 | 16.71 | 1.30 | 0.81 | 1.22 | −0.39 | 3.57 | 0.42 | 6.08 | c | S115 |
| 92 | 6:40:36.2 | 9:18:59.0 | 15.89 | 1.28 | 0.83 | 0.91 | −0.21 | 3.60 | 0.50 | 6.01 | xc | FX18 |
| 102 | 6:40:37.1 | 9:31:13.0 | 17.41 | 1.56 | 1.04 | 1.32 | −0.51 | 3.55 | 0.32 | 6.05 | x | FX20 |
| 106: | 6:40:37.3 | 9:35:46.0 | 8.24 | 1.33 | 0.62 | 0.47 | 2.58 | 3.68 | – | – | h | W69, V49, S134 |
| 110 | 6:40:37.8 | 9:34:57.0 | 16.50 | 1.02 | 0.89 | 1.18 | −0.29 | 3.57 | 0.37 | 5.89 | xhc | S141, H16, FX23 |
| 112 | 6:40:37.8 | 9:36: 0.0 | 15.20 | 2.56 | 0.44 | 1.52 | 0.18 | 3.58 | 0.31 | 4.98 | c | |
| 126 | 6:40:39.0 | 9:36: 3.0 | 16.19 | 1.30 | 0.87 | 1.18 | −0.17 | 3.57 | 0.34 | 5.75 | c | S144 |
| 129 | 6:40:39.3 | 9:34:48.0 | 16.46 | 1.42 | 1.01 | 1.05 | −0.28 | 3.57 | 0.37 | 5.88 | h | S147 |
| 134 | 6:40:40.0 | 9:35: 6.0 | 14.40 | 1.07 | 0.63 | 0.58 | 0.16 | 3.67 | 0.91 | 6.15 | xhp | W77, V54, S150, H18, FX26 |
| 145: | 6:40:40.8 | 9:27:57.0 | 16.32 | 1.21 | 0.79 | 0.78 | −0.46 | 3.61 | 0.74 | 6.70 | h | O89 |
| 149 | 6:40:41.1 | 9:33:60.0 | 15.88 | 0.50 | 0.76 | 0.67 | −0.34 | 3.63 | 0.82 | 6.67 | hcp | V57, S155, H22 |
| 157 | 6:40:41.9 | 9:22:57.0 | 16.01 | 1.06 | 0.59 | 0.71 | −0.45 | 3.65 | 0.90 | 7.12 | c | |
| 158 | 6:40:42.1 | 9:33:40.0 | 12.02 | 0.56 | 0.31 | 0.31 | 0.95 | 3.82 | 1.70 | 6.92 | hp | W84, V59, S163 |
| 161 | 6:40:42.4 | 9:25:15.0 | 16.15 | 2.12 | 1.20 | 1.17 | 0.00 | 3.55 | 0.23 | 4.82 | c | |
| 173 | 6:40:43.3 | 9:28:43.0 | 16.55 | 1.38 | 0.91 | 0.99 | −0.39 | 3.59 | 0.50 | 6.24 | h | O91 |
| 186 | 6:40:44.2 | 9:23:19.0 | 16.84 | 1.04 | 0.68 | 0.73 | −0.74 | 3.64 | 0.70 | 7.47 | c | |
| 188 | 6:40:44.5 | 9:32:29.0 | 18.51 | 0.61 | 1.30 | 1.45 | −0.74 | 3.52 | 0.22 | 6.12 | x | FX36 |
| 194 | 6:40:45.0 | 9:28:46.0 | 14.25 | 1.00 | 0.58 | 0.54 | 0.18 | 3.68 | 1.11 | 6.30 | hp | V65, M364 |
| 195 | 6:40:45.1 | 9:23:56.0 | 14.49 | 0.90 | 0.51 | 0.60 | 0.09 | 3.68 | 1.14 | 6.49 | p | V66 |
| 197 | 6:40:45.4 | 9:21:12.0 | 14.79 | 2.09 | 1.09 | 1.07 | 0.44 | 3.56 | 0.24 | 3.91 | c | |
| 200 | 6:40:45.9 | 9:17:59.0 | 16.67 | 1.09 | 0.86 | 1.02 | −0.45 | 3.59 | 0.55 | 6.37 | c | |
| 204 | 6:40:46.5 | 9:21:42.0 | 14.85 | 2.11 | 1.15 | 1.07 | 0.45 | 3.56 | – | – | c | |
| 207 | 6:40:46.8 | 9:32:33.0 | 17.67 | 2.13 | 0.75 | 1.25 | −0.79 | 3.57 | 0.60 | 6.94 | x | FX40 |
| 208 | 6:40:46.8 | 9:25:55.0 | 15.51 | 1.44 | 0.86 | 0.92 | −0.03 | 3.60 | 0.42 | 5.74 | h | O92 |
| 211 | 6:40:47.0 | 9:32:42.0 | 16.38 | 1.08 | 0.93 | 0.96 | −0.33 | 3.59 | 0.48 | 6.12 | xhc | W95, S186, H26, FX41 |
| 217 | 6:40:48.1 | 9:21:16.0 | 16.53 | 1.15 | 0.55 | 0.68 | −0.69 | 3.66 | 0.75 | 7.68 | c | |
| 219 | 6:40:48.2 | 9:36:41.0 | 16.30 | 1.62 | 0.81 | 1.14 | −0.27 | 3.58 | 0.42 | 5.95 | xc | W97, S191, FX44 |
| 221 | 6:40:48.5 | 9:32:55.0 | 17.01 | 1.42 | 0.82 | 0.94 | −0.64 | 3.60 | 0.71 | 6.92 | x | S193, FX45 |
| 223: | 6:40:48.6 | 9:22: 0.0 | 10.16 | 0.03 | −0.02 | 0.03 | 1.76 | 3.99 | 2.50 | 6.57 | xp | V73, FX46 |
| 224 | 6:40:48.6 | 9:36: 0.0 | 20.35 | −0.50 | 2.35 | 1.48 | −0.87 | 3.46 | 0.12 | 5.40 | h | O94 |
| 226 | 6:40:48.8 | 9:17:12.0 | 16.41 | 1.09 | 0.75 | 0.79 | −0.51 | 3.62 | 0.78 | 6.85 | c | |
| 230 | 6:40:49.2 | 9:23:51.0 | 15.99 | 1.26 | 0.84 | 0.81 | −0.29 | 3.61 | 0.58 | 6.24 | h | H29 |
| 250 | 6:40:51.4 | 9:28:46.0 | 16.05 | 1.12 | 0.79 | 0.81 | −0.33 | 3.61 | 0.64 | 6.39 | xhc | H34, FX50 |
| 262 | 6:40:53.6 | 9:30:41.0 | 11.67 | 0.51 | 0.26 | 0.30 | 1.08 | 3.83 | 1.78 | 6.87 | xp | W116, V83, S218, FX56 |
| 263 | 6:40:53.6 | 9:33:27.0 | 14.56 | 0.99 | 0.58 | 0.58 | 0.08 | 3.67 | 1.00 | 6.36 | xhp | W115, V82, S217, H35, FX54 |
| 264 | 6:40:54.0 | 9:29:53.0 | 17.16 | 1.46 | 0.96 | 0.99 | −0.61 | 3.58 | 0.59 | 6.64 | x | FX57 |
| 266 | 6:40:54.3 | 9:20: 5.0 | 11.81 | 0.54 | 0.30 | 0.31 | 1.03 | 3.82 | 1.71 | 6.91 | x | W118, FX58 |
| 269 | 6:40:55.2 | 9:17:53.0 | 15.50 | 1.10 | 0.62 | 0.74 | −0.22 | 3.64 | 0.84 | 6.54 | c | |
| 279 | 6:40:56.4 | 9:35:55.0 | 16.91 | 1.33 | 1.11 | 1.02 | −0.42 | 3.56 | 0.39 | 6.07 | hc | W123, S232, H40 |
| 281 | 6:40:56.6 | 9:30:17.0 | 15.90 | 1.28 | 1.02 | 1.28 | 0.07 | 3.55 | 0.24 | 4.75 | xc | W127, S235, FX63 |
| 290 | 6:40:57.7 | 9:30:52.0 | 16.49 | 1.49 | 0.88 | 1.04 | −0.36 | 3.58 | 0.48 | 6.15 | h | S238, O102 |
| 294 | 6:40:58.4 | 9:33:33.0 | 10.21 | −0.07 | −0.02 | 0.02 | 1.74 | 4.13 | – | – | xp | W132, V91, S242, FX65 |
| 297 | 6:40:58.6 | 9:36:15.0 | 17.06 | 1.37 | 0.98 | 1.68 | −0.21 | 3.53 | 0.20 | 5.05 | h | H42 |
| 298 | 6:40:58.7 | 9:30:59.0 | 13.78 | 1.10 | 0.61 | 0.57 | 0.40 | 3.67 | 0.95 | 5.87 | hp | V93, S244, S245, H43 |
| 299 | 6:40:58.8 | 9:28:54.0 | 16.80 | 1.20 | 0.95 | 1.29 | −0.32 | 3.56 | 0.33 | 5.86 | c | |
| 303 | 6:40:59.4 | 9:29:53.0 | 16.86 | 1.09 | 0.93 | 1.21 | −0.40 | 3.56 | 0.38 | 6.02 | hc | O105 |
| 304 | 6:40:59.5 | 9:28:45.0 | 16.14 | 1.24 | 0.78 | 0.92 | −0.32 | 3.60 | 0.57 | 6.27 | hc | H45 |
| 305 | 6:40:59.5 | 9:35:12.0 | 15.34 | 1.66 | 0.97 | 1.06 | 0.16 | 3.57 | 0.28 | 4.87 | xh | W136, S251, O104, FX71 |
| 306 | 6:40:59.9 | 9:28:51.0 | 15.76 | 1.42 | 0.65 | 0.80 | −0.29 | 3.63 | 0.76 | 6.52 | xc | FX73 |
| 309 | 6:41: 0.4 | 9:29:17.0 | 14.81 | 1.24 | 0.64 | 0.69 | 0.04 | 3.65 | 0.75 | 6.10 | x | S257, FX75 |
| 311 | 6:41: 0.6 | 9:24:12.0 | 10.20 | 0.05 | 0.04 | 0.06 | 1.71 | 3.96 | 2.50 | 6.55 | p | W138, V97 |
| 313 | 6:41: 0.9 | 9:32:46.0 | 13.44 | 1.30 | 0.71 | 0.73 | 0.64 | 3.63 | 0.50 | 4.84 | xh | W139, V98, S260, H47, FX78 |
| 314: | 6:41: 1.1 | 9:34:54.0 | 15.81 | 0.95 | 0.83 | 0.87 | −0.19 | 3.60 | 0.51 | 6.02 | h | O107 |
| 315 | 6:41: 1.3 | 9:34:10.0 | 14.58 | 1.18 | 0.65 | 0.65 | 0.12 | 3.65 | 0.76 | 6.03 | x | V100, S263, FX80 |
| 316 | 6:41: 1.4 | 9:28:14.0 | 10.69 | 0.02 | 0.04 | 0.08 | 1.50 | 3.95 | 2.39 | 6.64 | p | V102 |
| 321 | 6:41: 2.5 | 9:34:57.0 | 14.06 | 0.95 | 0.52 | 0.51 | 0.23 | 3.70 | 1.38 | 6.54 | x | W149, V105, S271, FX85 |
| 322 | 6:41: 2.5 | 9:35:14.0 | 15.30 | 1.22 | 0.69 | 0.71 | −0.12 | 3.64 | 0.72 | 6.27 | x | W150, S272, FX86 |
| 324 | 6:41: 2.7 | 9:27:25.0 | 9.17 | −0.14 | – | – | – | – | – | – | x | V108, FX87 |
| 328 | 6:41: 3.3 | 9:30: 6.0 | 16.82 | 1.72 | 0.93 | 1.36 | −0.31 | 3.55 | 0.31 | 5.82 | c | S278 |
| 330 | 6:41: 3.4 | 9:31:20.0 | 12.74 | 0.71 | 0.36 | 0.39 | 0.68 | 3.79 | 1.42 | 7.09 | xp | V109, S279, FX89 |
| 335 | 6:41: 3.6 | 9:27:41.0 | 16.07 | 1.05 | 0.80 | 0.83 | −0.33 | 3.61 | 0.61 | 6.34 | xc | FX90 |
| 338 | 6:41: 4.0 | 9:23:33.0 | 14.32 | 0.66 | 0.36 | 0.38 | 0.05 | 3.79 | – | – | p | V116 |
| 339 | 6:41: 4.0 | 9:35:22.0 | 16.47 | 1.40 | 0.92 | 1.12 | −0.29 | 3.57 | 0.38 | 5.91 | x | S282, FX93 |
| 340 | 6:41: 4.0 | 9:33: 3.0 | 10.08 | −0.09 | −0.03 | 0.00 | 1.80 | 4.16 | – | – | p | W157, V115, S283 |
| 342 | 6:41: 4.2 | 9:24:53.0 | 15.44 | 0.72 | 0.70 | 0.80 | −0.14 | 3.62 | 0.62 | 6.14 | hc | H49 |
| 349 | 6:41: 4.6 | 9:36:29.0 | 10.88 | 0.04 | 0.03 | 0.13 | 1.42 | 3.94 | 2.15 | 6.74 | xp | W159, V118, S290, FX96 |
| 351 | 6:41: 5.3 | 9:33:15.0 | 15.08 | 1.13 | 0.69 | 0.79 | −0.00 | 3.63 | 0.59 | 5.93 | x | W160, S296, FX98 |
| 353 | 6:41: 5.6 | 9:31: 2.0 | 15.41 | 1.38 | 0.84 | 0.94 | 0.01 | 3.60 | 0.41 | 5.69 | x | W162, S298, FX100 |

**Table 5.** (Continued)

| $N^1$ | $RA_{2000}$ h:m:s | $DEC_{2000}$ $^o$:':" | $V$ [mag.] | $B-V$ [mag.] | $V-R$ [mag.] | $R-I$ [mag.] | $Log(L_{bol})$ $[L_\odot]$ | $Log(T_{eff})$ $[^oK]$ | $M$ $[M_\odot]$ | $Log(Age)$ [years] | $Memb.^2$ | $Ident.^3$ |
|---|---|---|---|---|---|---|---|---|---|---|---|---|
| 355 | 6:41: 5.8 | 9:27:18.0 | 16.30 | 1.48 | 0.90 | 1.45 | −0.07 | 3.55 | 0.25 | 5.05 | c | |
| 356 | 6:41: 5.8 | 9:22:56.0 | 10.99 | 0.15 | 0.07 | 0.11 | 1.37 | 3.93 | 2.05 | 6.79 | p | W165, V121 |
| 358 | 6:41: 5.9 | 9:35:52.0 | 13.79 | 0.89 | 0.45 | 0.44 | 0.29 | 3.74 | 1.36 | 7.00 | hp | V120, S301, S302 |
| 360 | 6:41: 6.1 | 9:36:25.0 | 13.39 | 0.85 | 0.46 | 0.49 | 0.47 | 3.71 | 1.70 | 6.47 | xhp | W164, V122, S303, H53, FX101 |
| 361 | 6:41: 6.2 | 9:29:32.0 | 17.67 | 4.81 | 0.89 | 1.61 | −0.54 | 3.54 | 0.27 | 6.00 | x | FX103 |
| 364 | 6:41: 6.3 | 9:28:40.0 | 17.32 | 1.68 | 1.10 | 1.01 | −0.60 | 3.56 | 0.46 | 6.41 | h | H55 |
| 365 | 6:41: 6.5 | 9:35:47.0 | 14.06 | 0.74 | 0.37 | 0.35 | 0.15 | 3.79 | – | – | p | V123, S304 |
| 366 | 6:41: 6.7 | 9:34:47.0 | 16.14 | 1.29 | 0.84 | 0.98 | −0.27 | 3.59 | 0.48 | 6.06 | hc | W166, O112 |
| 367: | 6:41: 6.7 | 9:27:34.0 | 12.94 | 0.96 | 0.68 | 0.64 | 0.79 | 3.65 | 0.66 | 5.00 | hp | V124, H54 |
| 368 | 6:41: 6.7 | 9:29:26.0 | 17.45 | 1.11 | 0.83 | 1.07 | −0.75 | 3.59 | 0.69 | 7.03 | h | S306, O114 |
| 370 | 6:41: 6.9 | 9:27:50.0 | 14.91 | 1.10 | 0.74 | 0.80 | 0.09 | 3.62 | 0.51 | 5.72 | xc | FX105 |
| 371: | 6:41: 6.9 | 9:27:32.0 | 13.56 | 1.02 | −0.56 | 0.94 | 0.32 | 3.88 | – | – | h | H56 |
| 372 | 6:41: 7.1 | 9:31:20.0 | 17.75 | 1.55 | 1.00 | 1.31 | −0.67 | 3.55 | 0.37 | 6.35 | x | FX107 |
| 374: | 6:41: 7.3 | 9:25:56.0 | 15.15 | 1.30 | 0.77 | 0.86 | 0.04 | 3.61 | 0.46 | 5.71 | xh | O115, FX106 |
| 378 | 6:41: 7.8 | 9:30:43.0 | 15.61 | 1.16 | 0.70 | 0.66 | −0.26 | 3.64 | 0.86 | 6.63 | x | W175, S310, FX109 |
| 381 | 6:41: 8.8 | 9:23:44.0 | 14.73 | 1.28 | 0.79 | 0.85 | 0.21 | 3.61 | 0.42 | 5.51 | x | FX111 |
| 383 | 6:41: 8.9 | 9:30:11.0 | 15.79 | 0.78 | 0.78 | 0.83 | −0.23 | 3.61 | 0.57 | 6.16 | hc | S316, H58 |
| 385: | 6:41: 9.4 | 9:27:14.0 | 14.50 | 1.24 | 0.73 | 0.86 | 0.28 | 3.61 | 0.44 | 5.42 | x | V132, FX114 |
| 386 | 6:41: 9.6 | 9:27:53.0 | 10.21 | 0.11 | – | – | – | – | – | – | x | V130, FX115 |
| 391 | 6:41:10.1 | 9:28:35.0 | 16.00 | 0.32 | 0.82 | 0.80 | −0.31 | 3.61 | 0.60 | 6.30 | c | |
| 398 | 6:41:11.6 | 9:26:33.0 | 15.18 | 1.30 | 0.84 | 0.86 | 0.06 | 3.60 | 0.43 | 5.65 | xh | W183, H59, FX116 |
| 401 | 6:41:12.8 | 9:27:34.0 | 11.42 | 0.47 | 0.32 | 0.34 | 1.19 | 3.81 | 2.00 | 6.72 | xp | W189, V140, FX118 |
| 402 | 6:41:12.8 | 9:26:16.0 | 13.56 | 0.88 | 0.67 | 0.62 | 0.53 | 3.66 | 0.72 | 5.50 | hcp | V139, H61 |
| 404: | 6:41:13.1 | 9:28: 9.0 | 16.77 | 1.15 | 0.91 | 0.89 | −0.53 | 3.59 | 0.64 | 6.62 | x | FX124 |
| 406 | 6:41:13.2 | 9:26:11.0 | 14.31 | 1.14 | 0.73 | 0.74 | 0.30 | 3.63 | 0.52 | 5.51 | h | H62 |
| 407 | 6:41:13.9 | 9:26:42.0 | 16.48 | 1.34 | 0.87 | 1.00 | −0.38 | 3.59 | 0.51 | 6.23 | c | |
| 409 | 6:41:14.3 | 9:33:23.0 | 15.53 | 1.28 | 0.79 | 0.86 | −0.10 | 3.61 | 0.50 | 5.91 | x | W191, S335, FX126 |
| 411 | 6:41:14.7 | 9:32:38.0 | 16.87 | 1.69 | 1.09 | 1.40 | −0.22 | 3.54 | 0.24 | 5.35 | x | S336, FX127 |
| 413 | 6:41:14.9 | 9:26:46.0 | 16.74 | 1.21 | 0.95 | 1.09 | −0.40 | 3.57 | 0.42 | 6.09 | hc | H64 |
| 416 | 6:41:15.7 | 9:26:18.0 | 13.80 | 1.16 | 0.68 | 0.71 | 0.47 | 3.64 | 0.56 | 5.40 | x | V147, FX129 |
| 417 | 6:41:16.0 | 9:26:10.0 | 15.83 | 0.61 | 0.75 | 0.91 | −0.22 | 3.61 | 0.54 | 6.10 | c | |
| 418 | 6:41:16.5 | 9:29:54.0 | 15.30 | 1.42 | 0.91 | 1.00 | 0.11 | 3.59 | 0.34 | 5.28 | xh | V150, S343, M368, FX131 |
| 419 | 6:41:16.6 | 9:27:32.0 | 15.13 | 0.96 | 0.72 | 0.64 | −0.07 | 3.64 | 0.75 | 6.25 | hcp | V151, H65 |
| 420 | 6:41:16.7 | 9:36:23.0 | 17.60 | 1.38 | 1.08 | 1.41 | −0.52 | 3.54 | 0.27 | 5.99 | x | FX132 |
| 422 | 6:41:17.5 | 9:29:28.0 | 15.70 | 1.50 | 0.93 | 1.11 | 0.02 | 3.57 | 0.30 | 5.26 | x | S346, FX133 |
| 424 | 6:41:17.8 | 9:33:39.0 | 15.32 | 1.21 | 0.74 | 0.80 | −0.07 | 3.62 | 0.56 | 5.97 | x | W198, V152, S348, FX134 |
| 426 | 6:41:18.1 | 9:33:56.0 | 14.91 | 1.07 | 0.72 | 0.63 | 0.01 | 3.65 | 0.73 | 6.12 | xhp | W199, V153, S349, H68, FX135 |
| 427 | 6:41:18.2 | 9:31:32.0 | 18.43 | 1.55 | 1.00 | 1.46 | −0.86 | 3.54 | 0.30 | 6.48 | x | FX136 |
| 430: | 6:41:18.9 | 9:26:31.0 | 17.17 | 1.09 | 1.11 | 1.13 | −0.47 | 3.56 | 0.37 | 6.08 | h | H69 |
| 431 | 6:41:19.3 | 9:30:30.0 | 13.88 | 0.86 | 0.46 | 0.41 | 0.25 | 3.75 | 1.23 | 7.16 | p | V154, S352 |
| 434 | 6:41:19.5 | 9:31:46.0 | 14.31 | 1.18 | 0.67 | 0.66 | 0.24 | 3.65 | 0.68 | 5.78 | xp | V155, S353, FX138 |
| 440 | 6:41:20.9 | 9:33:38.0 | 15.23 | 1.20 | 0.78 | 0.78 | −0.03 | 3.62 | 0.53 | 5.87 | xh | W204, V159, S357, H70, FX141 |
| 441 | 6:41:21.0 | 9:32:16.0 | 17.77 | 1.61 | 0.93 | 1.21 | −0.76 | 3.56 | 0.48 | 6.69 | x | FX142 |
| 445 | 6:41:22.6 | 9:29:41.0 | 15.75 | 1.04 | 0.59 | 0.55 | −0.41 | 3.67 | 0.90 | 7.22 | h | S364, H71 |
| 447 | 6:41:22.8 | 9:27:28.0 | 12.67 | 0.71 | 0.41 | 0.42 | 0.73 | 3.76 | 1.67 | 6.85 | xp | W208, V164, FX146 |
| 449 | 6:41:23.6 | 9:33:58.0 | 11.32 | 0.34 | 0.21 | 0.20 | 1.21 | 3.88 | 2.00 | 6.79 | p | W209, V165, S366 |
| 451 | 6:41:24.3 | 9:21:39.0 | 13.32 | 0.54 | 0.28 | 0.29 | 0.42 | 3.83 | – | – | p | V166 |
| 452 | 6:41:24.3 | 9:32:47.0 | 16.73 | 1.50 | 0.94 | 1.21 | −0.34 | 3.56 | 0.36 | 5.92 | x | S369, FX148 |
| 453 | 6:41:24.6 | 9:26:24.0 | 13.38 | 0.73 | 0.40 | 0.37 | 0.43 | 3.78 | 1.30 | 7.20 | p | W210, V167 |
| 458 | 6:41:26.6 | 9:23:55.0 | 12.68 | 0.44 | 0.24 | 0.25 | 0.67 | 3.85 | – | – | p | V169 |
| 460 | 6:41:27.0 | 9:35: 8.0 | 14.37 | 1.01 | 0.57 | 0.56 | 0.14 | 3.68 | 1.06 | 6.33 | x | V170, S373, FX150 |
| 462: | 6:41:27.4 | 9:31:57.0 | 14.91 | 1.27 | 0.76 | 0.61 | 0.02 | 3.64 | 0.70 | 6.06 | h | S375, S376 |
| 470 | 6:41:30.9 | 9:26:59.0 | 13.56 | 0.83 | 0.56 | 0.60 | 0.48 | 3.67 | 1.01 | 5.81 | hcp | W215, V178, H72 |
| 473 | 6:41:32.8 | 9:19: 3.0 | 9.79 | 0.44 | 0.25 | 0.26 | 1.83 | 3.85 | – | – | x | W220, FX157 |
| 476 | 6:41:34.1 | 9:34:44.0 | 16.80 | 2.67 | 1.53 | 1.58 | 0.13 | 3.50 | – | – | c | S399 |
| 483 | 6:41:37.1 | 9:21: 0.0 | 11.58 | 0.62 | 0.32 | 0.34 | 1.13 | 3.81 | 1.92 | 6.77 | p | W224, V188 |
| 488 | 6:41:38.1 | 9:32:14.0 | 15.83 | 2.07 | 1.15 | 1.18 | 0.11 | 3.55 | 0.23 | 4.59 | c | S416 |
| 489 | 6:41:38.6 | 9:32:13.0 | 15.31 | 1.09 | 0.72 | 0.64 | −0.14 | 3.64 | 0.79 | 6.39 | h | V189, S417, H76 |
| 490 | 6:41:38.9 | 9:29:39.0 | 16.87 | 2.51 | 1.57 | 1.58 | 0.13 | 3.50 | – | – | c | S418 |
| 501 | 6:41:41.0 | 9:33:56.0 | 14.33 | 1.93 | 1.02 | 1.11 | 0.61 | 3.56 | – | – | cp | V192, S424 |
| 502 | 6:41:41.0 | 9:32:44.0 | 12.88 | 0.52 | 0.28 | 0.29 | 0.60 | 3.83 | 1.44 | 7.60 | p | V193, S426 |
| 505 | 6:41:42.8 | 9:25: 8.0 | 16.63 | 1.11 | 0.84 | 0.92 | −0.49 | 3.60 | 0.64 | 6.57 | hc | H78 |
| 508 | 6:41:43.2 | 9:27: 1.0 | 12.46 | 0.89 | 0.46 | 0.47 | 0.84 | 3.72 | 2.00 | 6.11 | p | W230, V199 |
| 511 | 6:41:44.2 | 9:25: 2.0 | 16.69 | 1.52 | 0.93 | 1.18 | −0.34 | 3.56 | 0.37 | 5.95 | h | O129 |
| 514 | 6:41:45.8 | 9:33: 3.0 | 15.09 | 2.04 | 1.05 | 1.14 | 0.34 | 3.56 | 0.23 | 4.13 | c | S443 |
| 520 | 6:41:47.7 | 9:34:10.0 | 14.53 | 1.23 | 0.69 | 0.73 | 0.19 | 3.63 | 0.58 | 5.70 | p | V204, S448 |

*Notes:* [1] Identification number (from Table 3), colons signal uncertain photometry.

[2] Membership criteria: 'c', this paper (see text); 'x', Flaccomio et al. (in prep.); 'h', Herbig (1954), Marcy (1980), Ogura(1984) or Sung et al. (1997); 'p', Vasilevskis et al. (1965) with membership probabilities $> 50\%$.

[3] Cross-identification; the one or two letter prefix indicates the original catalog while the number is the reference used by the authors of the catalog. The prefix stand for: "W", Walker (1956); "V", Vasilevskis et al. (1965);, "S", Sung et al. (1997); "O", Ogura (1984); "M", Marcy (1980); "H", Herbig (1954); "FX", Flaccomio et al. (in prep.).

## 4. Summary and Conclusions

The analysis of our CCD BVRI photometry in the southern part of the star-forming region NGC 2264 has lead to the identification of 24 previously unknown likely members of the association, on the basis of photometric color excesses. We have collected a critical compilation of the existing membership data for NGC 2264, building a sample which we show to be statistically complete for $M \gtrsim 0.6\,M_{\odot}$. Through star positions on the evolutionary tracks of D'Antona & Mazzitelli (1998), we have estimated their individual masses and ages, which we have then used to build an Initial Mass Function for the studied part of the region as well as to determine the star-formation history as a function of time in the region.

Our main result is that the IMF seems to differ from the field one (i.e. the Scalo 1986 IMF), due to the presence of a "bump" in the IMF at high masses

This features could point toward the presence of two somewhat distinct star-formation mechanisms being at work in NGC 2264, one for low-mass and one for high-mass stars (see e.g. Larson, 1986; Silk 1985; Lee & Chun, 1986). Following the discussion of Larson (1986) one may envision a scenario in which massive stars (such as the B1.5V star W178 which is at the center of the field studied here, or the O7V star S Mon) form at an early stage, and, due to the heating and/or strong ionization of the surrounding matter, prevent to some degree the formation of less massive stars, thus explaining the observed excess of high-mass stars in the IMF. The likehood of such an history of star formation will be greatly enhanced if the suggested difference in stellar age between samples of different mass will be confirmed with greater confidence.

We note that our conclusions are robust in the face of the existing uncertainty in the distance to NGC 2264. If we were to adopt the Pérez et al. (1987) distance of 950 pc, in place of the 760 pc (Sung et al. 1997) which was assumed throughout the present paper, the absolute age and mass estimates would change, thus shifting the mass at which the IMF shows a break, but the general conclusion about the presence of a bimodal IMF would not change.

A more complete survey of the region, both covering a wider area of the SFR and reaching down to fainter magnitudes in order to achieving completeness at lower masses, will be needed in the future to assess whether the bimodal structures of the IMF and the difference in characteristic ages of the high- and low-mass populations persist when a more complete census of the region is taken. Both deep optical and X-ray observations will be useful in this context.

*Acknowledgements.* EF, GM and SS acknowledge financial support from MURST (Ministero della Università e della Ricerca Scientifica e Tecnologica). EF thanks the "Università degli Studi di Palermo" for awarding a fellowship. We thank the referee D. Raboud for his useful comments that helped to improve this work.

## References

Adams M.T., Strom K.M., Strom S.E., 1983, ApJS 53, 893
Ashman K.M., Bird C.M., Zepf S.E., 1994, AJ 109, 2348
Bessel M.S., 1990, PASP 102, 1181
Bessel M.S., Stringfellow G.S., 1993, ARA&A 31, 433
Bertout C., Basri G., Bouvier J., 1988, ApJ 330, 350
Castelaz M. W., Grasdalen G., 1988, ApJ 335, 150
Code A.D., Davis J., Bless R.C., Hanbury Brown R., 1976, ApJ 203, 417
D'Antona F., Mazzitelli I., 1998, In: Micela G., Pallavicini R., Sciortino S. (eds.) Mem. Soc. Astron. Ital. Vol. 68., No. 4
Flaccomio E., 1996, Tesi di Laurea in Fisica, Università di Palermo
Hartigan P., Edwards S., Ghandour L., 1995, ApJ 452, 736
Herbig G.H., 1954, ApJ 119, 483
Kenyon S.J., Hartmann L.W., 1990, ApJ 349, 197
Lada C.J., Young E.T., Greene T.P., 1993, ApJ 408, 471
Landolt A.U., 1992, AJ 104, 340
Larson R.B., 1986, MNRAS 218, 409
Lee S.-W., Chun M.Y., 1986, JKAS 19, 51
Marcy G.W., 1980, AJ 85, 230
Margulis M., Lada C.J., Young E.T., 1989, ApJ 345, 906
Mermilliod J.-C., 1981, A&A 97, 235
Ogura K., 1984, PASJ 36, 139
Patten B.M., Simon T., Strom S.E., Strom K.M., 1994, In: Caillault J.P. (ed.) Cool Stars, Stellar System, and the Sun, A.S.P. Conf. Ser. 64, p. 125
Perez M.R., The P.S., Westerlund B.E., 1987, PASP 99, 1050
Raboud D., Mermilliod J.-C., 1998, A&A 333, 897
Rydgren A.E., 1979, AJ 84, 90
Sagar R., Piskunov A.E., Miakutin V.I., Joshi U.C., 1986, MNRAS 220, 383
Sagar R., Myakutin V.I., Piskunov A.E., Dluzhnevskaya O.B., 1988, MNRAS 234, 831
Scalo J.M., 1986, Fundamentals of Cosmic Physics, Vol 11., Gordon and Breach
Schmidt-Kaler T.H., 1982, In: Shaifers K.E., Voigt H.H. (eds.) Stars and Star Clusters. Landolt-Bornstein New Series, Volume 2b, Astronomy and Astrophysics, New York
Silk J., 1985, In: I.A.U. Symposium 115, p. 663
Simon T., Cash W., Snow T.P., 1985, ApJ 293, 542
Stahler S.W., 1985, ApJ 293, 207
Sung H., Bessell M.S., Lee S.-W., 1997, AJ 114, 2644
Vasilevskis S., Sanders W.L., Balz A.G.A., 1965, AJ 70, 797
Walker M.F., 1956, ApJS 2, 365
Walter F.M., Brown A., Mathieu R.D., Myers P.C., Vrba F.J., 1988, AJ 96, 297